Biophysical Journal
Article

Biophysical Society

Temperature-Induced Catch-Slip to Slip Bond Transit in *Plasmodium falciparum*-Infected Erythrocytes

Ying Bena Lim,[1,2] Juzar Thingna,[2,3,4] Fang Kong,[2,5] Ming Dao,[2,5,6] Jianshu Cao,[2,3,*] and Chwee Teck Lim[1,2,7,*]
[1]Department of Biomedical Engineering, National University of Singapore, Singapore; [2]Singapore-Massachusetts Institute of Technology Alliance for Research and Technology Centre, Infectious Diseases IRG, Singapore; [3]Department of Chemistry, Massachusetts Institute of Technology, Cambridge, Massachusetts; [4]Center for Theoretical Physics of Complex Systems, Institute for Basic Science, Daejeon, Republic of Korea; [5]School of Biological Science, Nanyang Technological University, Singapore; [6]Department of Material Science and Engineering, Massachusetts Institute of Technology, Cambridge, Massachusetts; and [7]Institute for Health Innovation and Technology (iHealthtech), National University of Singapore, Singapore

ABSTRACT *Plasmodium falciparum* malaria-infected red blood cells (IRBCs), or erythrocytes, avoid splenic clearance by adhering to host endothelium. Upregulation of endothelial receptors intercellular adhesion molecule-1 (ICAM-1) and cluster of differentiation 36 (CD36) are associated with severe disease pathology. Most in vitro studies of IRBCs interacting with these molecules were conducted at room temperature. However, as IRBCs are exposed to temperature variations between 37°C (body temperature) and 41°C (febrile temperature) in the host, it is important to understand IRBC-receptor interactions at these physiologically relevant temperatures. Here, we probe IRBC interactions against ICAM-1 and CD36 at 37 and 41°C. Single bond force-clamp spectroscopy is used to determine the bond dissociation rates and hence, unravel the nature of the IRBC-receptor interaction. The association rates are also extracted from a multiple bond flow assay using a cellular stochastic model. Surprisingly, IRBC-ICAM-1 bond transits from a catch-slip bond at 37°C toward a slip bond at 41°C. Moreover, binding affinities of both IRBC-ICAM-1 and IRBC-CD36 decrease as the temperature rises from 37 to 41°C. This study highlights the significance of examining receptor-ligand interactions at physiologically relevant temperatures and reveals biophysical insight into the temperature dependence of *P. falciparum* malaria cytoadherent bonds.

SIGNIFICANCE Malaria is a mosquito-borne disease. The deadliest species of malaria is believed to cause death by obstructing blood flow in the vessels of vital organs. This process occurs as sticky infected red blood cells (IRBCs) accumulate in host vasculature. Studies that investigated IRBC-vascular protein interactions were performed mostly at room temperature. Considering that malaria patients often experience cyclic fever, we probed these bonds at body and febrile temperatures. We discovered that temperature can change the way IRBCs bind to vasculature. We also found that the propensity for IRBCs to form bonds with vessel wall proteins decreases as the temperature rises. Our work provides insights into the temperature sensitivity of these bonds and highlights the significance of conducting adhesion studies at physiologically relevant temperatures.

INTRODUCTION

There were 216 million malaria infections and 445,000 related deaths in 2016 (1). *Plasmodium falciparum* (*P.falciparum*) alone contributed to 99.7% of the infections in Africa, where 90% of global cases occurred (1). During the 48-h asexual life cycle of the parasite, its host develops clinical symptoms ranging from chills and fever (2) to severe symptoms such as severe anemia, multiple organ failure, impaired consciousness, and even death (3,4). High parasitemia and sequestration—the accumulation of infected red blood cells (IRBCs) cytoadhered in microvasculature throughout the body—are likely causes of these severe symptoms (2).

Cytoadhesion is believed to be a strategy used by the parasite to evade the host's splenic clearance system, which removes impaired or old red blood cells (RBCs) (5,6). It involves the adhesion of parasite-exported ligands

Submitted June 3, 2019, and accepted for publication November 12, 2019.
*Correspondence: jianshu@mit.edu or ctlim@nus.edu.sg
Editor: Elizabeth Rhoades.
https://doi.org/10.1016/j.bpj.2019.11.016

on the IRBC membrane to receptors on the endothelial cells of its human host (7). The parasite-exported proteins on *P. falciparum* IRBCs have been shown to bind to endothelial receptors intercellular adhesion molecule-1 (ICAM-1) in cerebral malaria (8,9) and cluster of differentiation 36 (CD36) in uncomplicated and severe malaria (10). Thus, these two molecules are most studied against *P. falciparum* IRBCs (7). Interestingly, experiments performed in flow chamber systems showed that ICAM-1 initiates the rolling of IRBCs on the endothelium, whereas CD36 arrests the motion of IRBCs (11,12). These findings suggest that IRBC-ICAM-1 interacts via transient adhesion, whereas IRBC-CD36 bonds form firm adhesion. This contrast in adhesion phenotype could potentially originate from the different biophysical nature of IRBC-receptor interactions (13). Specifically, IRBCs and ICAM-1 form catch-slip bonds, displaying catch bond behavior (i.e., bonds that break slower with increasing force (3∼15 pN)) before transiting to slip bonds (13). On the other hand, IRBCs and CD36 bind via slip bonds, which break faster with increasing force (13). Although these in vitro adhesion studies deepened our understanding of sequestration in *P. falciparum*, the experiments were all conducted at room temperature (11–13).

The *P. falciparum* host often experiences malaria paroxysm, during which, temperatures can rise to 41°C for 2–6 h (14). This periodic febrile response occurs as a result of the bursting of mature parasites, otherwise known as schizonts (14). Although the life cycle of *P. falciparum* is 48 h, febrile response is usually irregular (14). Febrile temperatures have been demonstrated to not only stiffen late stage IRBCs (15) but also enhance and accelerate the expression of adhesion ligands on the host membrane (16,17). Moreover, studies have revealed that temperature can modify antibody-antigen binding kinetics (18,19) and protein structure (20,21). It is hence likely that temperature variations during malaria infection can alter the binding kinetics of IRBC-receptor interactions and their protein structures.

This work employed biophysical tools to probe how temperature could affect IRBC-receptor binding kinetics. Measurements were performed at both single and multiple bond levels at body and febrile temperatures (i.e., 37 and 41°C, respectively). In doing so, we answer the following questions: How does IRBC binding to each endothelial receptor vary with temperature? How can these variations affect the roles that ICAM-1 and CD36 play in stabilizing IRBC adhesion? Single bond lifetimes were measured at various tensile forces to determine bond lifetime versus force relationships. We then used a flow chamber assay to extract association rates at these temperatures through a cellular stochastic model. Surprisingly, the nature of IRBC-ICAM-1 interactions transited from a catch-slip bond at 37°C to a slip bond at 41°C. Binding affinities of both IRBC-ICAM-1 and IRBC-CD36 were also found to decrease as the temperature rose from 37 to 41°C. Our findings emphasize the importance of studying IRBC adhesion at physiologically relevant temperatures.

MATERIALS AND METHODS

Parasite culture

All experiments were conducted using the *P. falciparum* 3D7 knob-positive strain that was adapted for laboratory culture (22). The malaria culture medium (MCM) was prepared using the following: MilliQ water, RPMI 1640 (Invitrogen, Carlsbad, CA), 0.5% AlbuMAX II (Invitrogen), 50 μg/mL hypoxanthine (Sigma-Aldrich, St. Louis, MO), 2 mM L-glutamine (Sigma-Aldrich), and 25 μg/mL gentamycin (Gibco, Thermo Fisher Scientific, Waltham, MA) (23). MCM was sterilized via filtration in a biosafety cabinet and kept at 4°C. Cultures were maintained at 2.5% hematocrit with 1–5% parasitemia and incubated at 37°C with 5% CO_2 and 3% O_2 gas composition. When the IRBCs were predominantly in the ring stage, parasites were synchronized using 5% D-sorbitol (Sigma-Aldrich) (23). Parasitemia was assessed by examining Giemsa-stained blood smears under a microscope at 100× magnification.

Purification of schizonts

Schizonts, or late stage IRBCs, possess paramagnetic iron in the hemozoin, which enables them to be purified from the culture via magnetic-activated cell sorting (24). The LD column (Miltenyi Biotec, Bergisch Gladbach, Germany) and SuperMACS II separator (Miltenyi Biotec) were used to isolate schizonts. After mounting the LD column onto the SuperMACS II separator, MCM was added for priming. The culture suspension was then introduced while the column was under the influence of the magnetic field from the separator. Next, the column was rinsed with MCM, at least twice, to rinse away uninfected RBCs and ring stage IRBCs. The column was then infused with MCM and removed from the separator. Thereafter, a plunger was used to elute the late IRBCs into a clean collection tube. Schizonts were retrieved from the cell pellet after centrifuging the cell suspension at 600 × *g* for 5 min at maximum acceleration and low deceleration. The last step was to resuspend the pellet in MCM to the desired concentration for experiments. The purity of late IRBCs attained was usually above 80%.

Selection of ICAM-1 adhesion phenotype

To ensure that IRBCs could adhere to both ICAM-1 and CD36 at the same time, *P. falciparum* 3D7 parasites were selected for the ICAM-1 adhesion phenotype. A 22-mm diameter glass coverslip was first rinsed with 70% ethanol followed by MilliQ water. Next, the coverslip was air dried and placed in a six-well plate. After being plasma treated for 10 min, the six-well plate was then exposed to ultraviolet radiation for 30 min in the biosafety cabinet. The coverslip was then coated with 100 μL of 100 μg/mL recombinant human ICAM-1 protein (Sino Biological, Beijing, China). Subsequently, the six-well plate was sealed with parafilm and incubated at 4°C overnight. The ICAM-1 coated coverslip was washed with 1× phosphate-buffered saline (PBS) on the next day. To reduce nonspecific adhesion, 1% bovine serum albumin (BSA) (Miltenyi Biotec) was then added to the coverslip at room temperature for 30 min. After rinsing with 1× PBS, magnetically purified IRBCs were added to the coverslip, and the six-well plate was placed in the malaria culture incubator for 1 h. RPMI was then used to rinse away the unbound IRBCs for more than five times. Next, 250 μL of RBC pellet and 5 mL of MCM were added into the well and placed into the incubator. The culture was transferred to a T25 culture flask with 10 mL fresh MCM the next day. A second round of selection was conducted when the parasitemia of the selected culture is above 5%. The twice-selected culture was expanded, aliquoted, and frozen for future experiments.

Force-clamp spectroscopy sample holder fabrication

Customized sample holders were fabricated to contain small volumes of fluid. Each sample holder is made up of a polydimethylsiloxane (PDMS) ring bound to a 30-mm diameter coverslip. The PDMS prepolymer base and cross-linking agent (Dow Corning, Midland, MI) were first mixed 10:1 by weight and poured into a 140-mm diameter petri dish to a height of 5 mm. Next, the petri dish was placed into a desiccator connected to a vacuum pump to remove all bubbles. The PDMS was then left to cure in the oven at 80°C for 2 h. Thereafter, the PDMS slab was peeled out of the petri dish. Rings of 25-mm internal diameter and 32-mm outer diameter were then drawn on the PDMS slab with a marker. After covering the entire PDMS slab with traces of rings, a knife was used to cut the rings out. The underside of each ring and an equal number of coverslips were plasma treated for 10 min before alignment. Finally, the bonded sample holders were placed in the oven for 2 h at 80°C.

Force-clamp spectroscopy sample preparation

The sample used for our single bond force-clamp spectroscopy experiments was prepared by immobilizing purified late IRBCs on the sample holder. The sample holder was first rinsed with 70% ethanol followed by MilliQ water. After air drying, it was plasma treated for 10 min. Thereafter, 300 μL of 50 μg/mL *Phaseolus vulgaris*-erythroagglutinin (Vector Laboratories, Burlingame, CA) was added and left at room temperature for 1 h. *P. vulgaris*-erythroagglutinin is known to adhere well to glycophorin on human RBCs (25). Next, the sample holder was washed thrice with 1× PBS. Magnetically isolated schizonts were then added and incubated at room temperature for 30 min. MCM was subsequently used to rinse away any unbound or loosely bound IRBCs. Finally, the sample holder was filled with 1% BSA in 1 mL MCM before placing into the substrate holder of the heating system.

Functionalization of AFM tip

Single bond force-clamp spectroscopy experiments were conducted using the B-lever of gold-coated Bio-Lever AFM tips (Olympus, Tokyo, Japan). AFM tips were functionalized as described in an earlier publication (13). It was noted that the adhesion frequency of receptors to IRBCs rose significantly with temperature, probably as a result of increased trafficking of PfEMP1 (16). Consequently, the concentrations of reagents used had to be optimized to maintain an adhesion frequency of less than 20% to ensure that most adhesion events observed were mediated by single bonds (26,27).

Briefly, the tip was treated with plasma for 10 min before placing in a 10-μL drop of 0.5 mg/mL BSA-biotin (Sigma-Aldrich) overnight in a humidified chamber at 4°C. The tip was next immersed in 10 μL of 10 μM streptavidin (Thermo Fisher Scientific) for 30 min before another 30 min in 200 μL of 10 mg/mL *N*-hydroxysuccinimide-polyethylene glycol 4-biotin (Thermo Fisher Scientific). Thereafter, the tip was incubated for 1 h with either 10 μL of human recombinant ICAM-1 protein—5 μg/mL for force-clamp spectroscopy at 37°C and 2.5 μg/mL for 41°C—or CD36 (Sino Biological)—2 μg/mL for both temperatures. The final step was to block excess amine groups that had been activated using 1 mg/mL glycine (Sigma-Aldrich) for 30 min. Each step was followed by washing with 1× PBS to remove any unbound reagent. Validation of the functionalization protocol can be found in Supporting Materials and Methods, Section 1.

Force-clamp spectroscopy protocol

The heating system described in Supporting Materials and Methods, Section 2 was switched on for 30 min before each experiment. Subsequently, the filled sample holder was placed into the substrate holder. The thermocouple connected to the thermometer (EasyView 11A Type K Thermometer, Extech Instruments, Waltham, MA) was then placed in direct contact with the cover glass of the sample holder and fixed in position with masking tape. Thereafter, the functionalized AFM tip was mounted onto the JPK NanoWizard II (Bruker, Billerica, MA), and the system was left to equilibrate to the desired temperature.

The B-lever was calibrated after the temperature had stabilized for 20 min using the in-built thermal fluctuation analysis of the JPK SPMControl Software v.4 (Bruker). Calibrated spring constants ranged from 2 to 12 pN/nm, which were within the manufacturing range. The cantilever was recalibrated at 1-h intervals to account for any effect of thermal drift. Temperature was monitored regularly throughout the experiment to ensure that the substrate is ± 1°C of the desired temperature.

Force-clamp spectroscopy was conducted using the methods documented in an earlier publication (13). It was observed that the effects of fluid drag on the AFM tip was very significant when experiments were conducted at 37 and 41°C. Consequently, the approach and retract speeds were reduced. As adhesion frequency was also much higher at these temperatures, the set point and contact time were also reduced to maintain an adhesion frequency of less than 20% (26,27). Each cycle began by approaching the IRBC at a set point of 15–30 pN and constant speed of 0.5 μm/s. The tip was then held at the constant set point for 20–50 ms for the receptors to interact with the IRBC ligands. Next, it was retracted to 0–30 pN at 200 nm/s and held at a constant force for 10 s for any formed bonds to break. The final step was to retract the tip by 3 μm at 2 μm/s to break any other remaining bonds before probing the next location on the IRBC membrane in a grid-like manner. Throughout this cycle, the broken bonds remained separate, and rebinding did not happen. In addition, we noted that the immobilized schizont IRBCs degraded with time at 41°C, an observation similar to another study that measured IRBC membrane stiffness at febrile temperature (15). AFM tips were also more prone to being fouled by cellular debris at 41°C. These situations limited the time window for obtaining data to ~3 h.

All the raw data files were analyzed using the JPK SPM data processing software (Bruker) as detailed in our previous publication (13). The single bond lifetime and breaking force measurements were all pooled and binned. There were at least 50 single bond lifetimes per bin for both IRBC-ICAM-1 and IRBC-CD36 interactions measured at 37°C and at least 30 lifetimes per bin at 41°C.

Determining the order of kinetics

Our experiments only involve the dissociation of single bonds and do not involve the reassociation of bonds. If the IRBC-receptor adhesion is of first order kinetics, the analytical solution to the probabilistic model for small system kinetics (28) will be as follows:

$$P = \frac{e^{-k_{off}t}}{Z}. \quad (1)$$

In this expression, P is the probability of detecting a bond between the IRBC and the receptor on the AFM tip at time t. The probability P stems from the random nature of bond dissociation (29). The parameter k_{off} is the dissociation rate, and Z is a normalization factor. The natural log of the number of dissociation events with a single bond lifetime greater than t was plotted against t to determine the survival probabilities of the bonds in each force bin. For a first order kinetics IRBC-receptor interaction, the graph should show a straight line with a negative gradient for each force bin. The lifetime of the single bond can hence be expressed as the inverse of the dissociation constant k_{off}.

Theoretical models for fitting single bond force-clamp spectroscopy data

The theoretical models used for fitting the single bond force-clamp spectroscopy data are the same as that described in our earlier publication

(13). For slip bonds, we use the following model proposed by Bell (30) and later supported theoretically by Evans and Ritchie (31):

$$k_{off}^{s} = k^{s} e^{\beta F x_0}. \quad (2)$$

The parameter k^s is the spontaneous dissociation rate (i.e., $k_{off}^{s} = k^{s}$) when the constant force F applied on the single bond is zero. The inverse temperature$\beta = (1/k_B T)$, where k_B is the Boltzmann constant, and T denotes the temperature. Last, x_0 is the stress-free bond length of the receptor-ligand interaction.

For catch-slip bonds, the dissociation rate was expressed by Dembo et al. (32) and rewritten in the following form based on the underlying assumption that the receptor-ligand bond is a Hookean spring:

$$k_{off}^{c} = k^{c} e^{\beta(F-F_0)^2 \xi}. \quad (3)$$

The force at which the bond transits from catch to slip bond behavior $F_0 = -(\kappa - \kappa_{ts})(\lambda - \lambda_{ts})$, and the inverse effective spring constant $\xi = (1/2(\kappa - \kappa_{ts}))$, with κ being the stiffness of the Hookean spring, λ its stress-free length, and the subscripts *ts* denoting the parameters for the transition state. The parameter k^c is the dissociation rate when $F = F_0$. Catch-slip bond behavior can also be described by other existing models (33,34), of which the two-pathway model can be backed by Kramers' rate theory (35). Recent studies have shown that the force-dependent entropic extension fluctuation of molecules can affect whether a receptor-ligand interaction behaves as a catch or slip bond while also requiring the existence of only one bond state (36,37). In this work, there is no structural basis to account for the conformational changes at submolecular levels. It is thus not possible for us to determine which one of these several models apply to the IRBC-ICAM-1 bond pair (33). Hence, our aim is not to identify the mechanism of the catch-slip bond but, instead, to demonstrate the presence of catch-slip bond behavior. Resultantly, we chose the model by Dembo et al. described above as it involves the least number of independent parameters to describe a Gaussian, which we observed from our 25°C experimental data (13).

If the bonds formed between IRBCs and each receptor follow first order kinetics, Eqs. 2 and 3 can be written in terms of the single bond lifetime τ as follows:

$$\tau = \frac{1}{k^{s}} e^{-\beta F x_0}, \quad (4)$$

and

$$\tau = \frac{1}{k^{c}} e^{-\beta(F-F_0)^2 \xi}. \quad (5)$$

Functionalization of microfluidic channel

The microfluidic channels used were 1.5-cm long with a rectangular cross section—500 μm wide × 27.6 μm high—and were fabricated using standard soft lithography methods (13). These channels were coated with either ICAM-1 or CD36 recombinant protein as documented by Xu et al. (38). First, 70% ethanol was used to prime the channel to prevent the formation of bubbles. The channel was then rinsed with 1× PBS before introducing either ICAM-1 or CD36. For consistency with the flow assays conducted at 25°C (13), the same concentrations of ICAM-1 (50 μg/mL) and CD36 (2 μg/mL) were used. Thereafter, the channel was kept overnight at 4°C in a humidified chamber. The protein solution was rinsed with 1× PBS the following day. To minimize nonspecific adhesion, the channel was filled with 5% BSA in PBS for 1 h at room temperature. The channel was then rinsed with 1× PBS before filling it with MCM for experiments. Validation of the functionalization protocol can be found in Supporting Materials and Methods, Section 3.

Flow assay protocol

The heating system (Supporting Materials and Methods, Section 4) was warmed up 10 min before the experiment. Next, the serological pipette was aligned vertically to the table using a spirit level. Thereafter, the channel was stuck onto the heating stage and connected to the serological pipette. The volume of water in the serological pipette was then fine-tuned using the syringe such that there was no flow in the channel. The thermocouple connected to the thermometer was subsequently inserted into the inlet reservoir and fixed in position (Supporting Materials and Methods, Section 4). The temperature of the heating stage was then adjusted to attain the desired substrate temperature. Enriched IRBCs were added into the inlet reservoir before noting the height of the water column in the serological pipette corresponding to the equilibrium pressure. This is the pressure at the outlet that matches the inlet pressure such that there is no flow within the channel. The observation field was then adjusted to the midpoint along the length of the microfluidic channel. The setup was left on the heating stage for 20 min after the set temperature was reached to provide the cells sufficient time to react to the temperature (15).

Subsequently, the experiment was performed as described in our previous work (13). The same experimenter ran all the flow assays for regularity in identifying adhesion events. The temperature was monitored regularly during the experiment to ensure that the substrate was 37 ± 1 or 41 ± 1°C. There were at least 20 cellular lifetimes per shear rate for both IRBC-ICAM-1 and IRBC-CD36 interactions measured at 37 and 41°C. Like the single bond force-clamp spectroscopy experiments, late stage IRBCs degraded with time at 41°C. The time window for conducting experiments for each protein-coated channel was resultantly limited to 2 h because of the accumulation of cellular debris on the substrate. Details of the flow calculations are presented in Supporting Materials and Methods, Section 5.

Theoretical models for the fitting of multiple bond flow assay data

The theoretical models used to connect the single bond force-clamp spectroscopy findings to the multiple bond flow assay were the same as that in another publication (13). In summary, the contact area of the cell to the channel was simplified to be a rectangle of length a and width b (39). It was assumed that all the adhesion kinetics happen within a small region known as the rupture area—a rectangular part of the contact area of length c and width b. Assuming that the IRBC is either attached or detached—rolling velocity $v \approx 0$—mechanical equilibrium equations were solved to attain the tension $\underline{Q}$ experienced by each bond (40):

$$Q \approx \frac{28.4\pi r^3}{\sigma a b c} \tau_w. \quad (6)$$

The parameter σ is the effective density of binding molecules, which depends on the dominant ligand or receptor, r is the radius of the IRBC, and τ_w is the wall shear stress.

Considering that the expression of tension Q in Eq. 6 is not restricted by the type of bond, it can thus be used to describe both IRBC-ICAM-1 catch-slip bonds and IRBC-CD36 slip bonds. The binding of a cluster can be visualized as a chain reaction (41,42), as follows:

$$N \rightleftarrows N-1 \rightleftarrows \cdots \rightleftarrows 2 \rightleftarrows 1 \rightarrow 0.$$

The average lifetime of a single bond can be obtained by computing the average turnover time (43,44) for the chain using the following:

$$\tau_N^x = \frac{1}{k^x} \frac{(N-1)!}{N} \left(\frac{k_{on}^x}{k^x}\right)^{N-1} f_N^x, \quad (7)$$

which is a simplified expression because shear stress τ_w is low ($\Rightarrow Q$ is low). This expression is consistent with the findings attained by Erdmann and Schwarz (42).

The function f_N^x depends on the number of PfEMP1 proteins per single knob N in the rupture area and the type of bond—$x = s$ represents slip bond, whereas $x = c$ denotes catch-slip bond. For simplicity, we assumed that bond association rate k_{on}^x for both catch-slip and slip bonds are independent of force F, similar to Bell (30). For slip bonds,

$$f_N^s = \exp\left[-Q\beta x_0 \sum_{i=1}^{N} \frac{1}{i}\right], \tag{8}$$

and for catch-slip bonds,

$$f_N^c = \exp\left[-\beta\left(\sum_{i=1}^{N} \frac{Q}{i} - F_0\right)^2 \xi\right]. \tag{9}$$

Eqs. 8 and 9 are both coarse-grained measures of the association rates averaged over the range of forces experienced during the flow experiments. The inherent stochasticity of bond association and dissociation are not reflected in these equations as a result of the averaging process. Using Eqs. 6, 7, 8, and 9, the lifetime of the IRBC was determined. It is apparent that the lifetime of the cell is dependent on the single bond parameters (k^x, βx_0, $\beta\varepsilon$, and F_0), demonstrating the relation between the single bond force-clamp spectroscopy to the multiple bond flow assay.

Ethics

Human erythrocytes were obtained from donors under the approval of the National University of Singapore Institutional Review Board. Informed written consent was obtained from donors.

RESULTS

Single bond force-clamp spectroscopy at 37 and 41°C

Single bond force-clamp spectroscopy studies the dissociation, or breaking, of a bond between a single receptor-ligand pair (13). The ligand in this study refers to *P. falciparum* erythrocyte membrane protein-1 (PfEMP1) expressed on the IRBC membrane (Supporting Materials and Methods, Section 6). The receptor that binds to PfEMP1 in our experiments is either ICAM-1 or CD36. Atomic force microscopy (AFM) is used for the single bond force-clamp spectroscopy measurement (45,46). To perform experiments at physiologically relevant temperatures, a heating system was integrated with the AFM setup (Supporting Materials and Methods, Section 2). The temperature of the substrate was kept within ±1°C of the set temperature—37 or 41°C.

A graphical presentation of each probing cycle is illustrated in Fig. 1 *a*, whereas a typical force curve is presented in Fig. 1 *b*. The functionalized AFM tip moved toward and away from the target cell according to the height profile (*blue*) while the corresponding forces were recorded (*red*). Only force curves in which there was only one breaking event during the force clamp were processed (Fig. 1; only

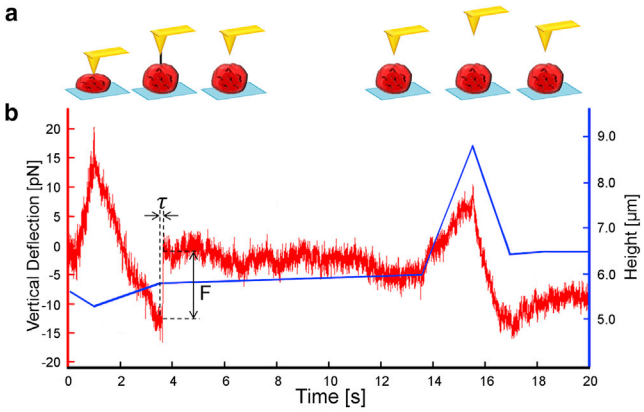

FIGURE 1 Single bond force-clamp spectroscopy at physiological temperatures. (*a*) Shown is an illustration of experimental procedure corresponding to different stages in (*b*). The black line between the AFM tip and the cell represents a single IRBC-receptor bond. (*b*) Shown is the processed force curve (*red*) portraying the dissociation of a single bond (at t ≈ 3.8 s) as the functionalized AFM tip moves according to the height profile (*blue*). The AFM tip deflected as the tip moved up and down between t ≈ 14 s and t ≈ 17 s because of viscous forces from moving in the surrounding medium. The single bond breaking force F and single bond lifetime τ can be measured from the force curve as indicated by the arrows. To see this figure in color, go online.

breaking event occurred at t ≈ 3.8 s). Even after the bond broke, the AFM tip still deflected as it moved up (to break any other unbroken bonds in the event that multiple bonds were formed) and down (for the next probing cycle) between t ≈ 14 s and t ≈ 17 s because of the viscous forces arising from moving in the surrounding medium. The force F and single bond lifetime τ were measured as illustrated by the arrows. All data were pooled and binned before theoretical analyses.

Both IRBC-ICAM-1 and IRBC-CD36 bonds followed first order kinetics as bond survival probability decreased exponentially with time at both 37 and 41°C (Fig. 2, *c–f*). The single bond lifetime τ versus force data of IRBC-ICAM-1 bond force-clamp spectroscopy demonstrated that the overall nature of the bond at 37°C was similar to that at room temperature (13) (Fig. 2, *a* and *b*) (i.e., IRBC-ICAM-1 are catch-slip bonds (Fig. 2 *c*) and IRBC-CD36 are slip bonds (Fig. 2 *d*)). Although IRBC-CD36 remained as a slip bond at 41°C (Fig. 2 *f*), it was intriguing to observe that IRBC-ICAM-1 transited from catch-slip behavior (Fig. 2 *c*) toward a slip bond (Fig. 2 *e*).

We validated this transition by performing the ANOVA test as well as a goodness of fit test at 37 and 41°C for catch-slip bond, ideal bond (lifetime is independent of the force acting on the bond (47)), and slip bond models (Table 1). For the ANOVA test, a high F ratio coupled with a low p value indicates that the model is a better fit. As seen in Table 1, the IRBC-ICAM-1 data fit the best into the catch-slip bond model at 37°C (F ratio = 627.12, p value = 7.02×10^{-8} versus slip bond: F ratio = 379.62, p value = 4.82×10^{-7}) and the slip bond model at 41°C

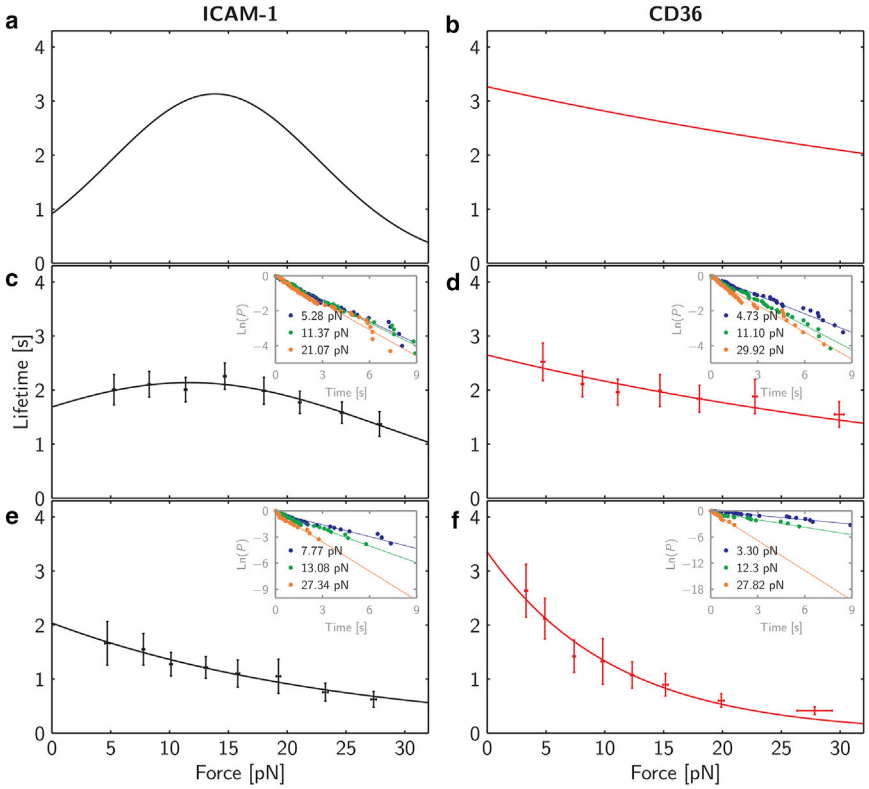

FIGURE 2 Results from single bond force-clamp spectroscopy experiments conducted at 25, 37, and 41°C. Single bond lifetime τ against force of IRBC-ICAM-1 and IRBC-CD36 bonds at 25°C (*a* and *b*) (13), 37°C (*c* and *d*), and 41°C (*e* and *f*) fitted to their corresponding catch-slip and slip bond models (*solid lines*). Single bond lifetimes are plotted as mean ± SEM. Insets are plots of the survival probability P of IRBC-ICAM-1 and IRBC-CD36 interactions at 37°C (*c* and *d*) and 41°C (*e* and *f*) fitted to straight lines (*solid lines*) via least-square method (bi-square weights) to indicate first order kinetics. To see this figure in color, go online.

(F ratio = 1213.28, p value = 1.50×10^{-8} versus catch-slip bond: F ratio = 244.58, p value = 7.66×10^{-6}). The subsequent test was based on the Akaike information criterion (AIC) and Bayesian information criterion (BIC), which are criteria for model selection based on the likelihood function such that lower AIC and BIC values indicate fewer variables, better fit, or both (48). Additionally, the closer R^2 and adjusted R^2 are to 1, the better the fit. Similarly, the tests indicated that at 37°C, the IRBC-ICAM-1 interaction is governed by a catch-slip bond (AIC = −7.21, BIC = −6.42, R^2 = 0.9968, adjusted R^2 = 0.9952) instead of a slip bond (AIC = 0.23, BIC = 0.47, R^2 = 0.9922, adjusted R^2 = 0.9895). At 41°C, the IRBC-ICAM-1 data fit better in the slip bond model (AIC = −16.40, BIC = −16.16, R^2 = 0.9975, adjusted R^2 = 0.9967) than in a catch bond model (AIC = −6.32, BIC = −6.00, R^2 = 0.9932, adjusted R^2 = 0.9892). Although it has been shown that interaction between complementary DNAs can be affected by temperature (49), it is interesting that temperature can also affect the way a receptor-ligand bond responds to tensile forces.

Fig. 2 and Table 2 revealed that single bond lifetimes of both IRBC-receptor interactions were reduced at febrile temperature. IRBC-ICAM-1 bonds tend to break faster within the force range measured as the temperature rose from 37 to 41°C (Fig. 2, *c* and *e*). At 37°C, k^c of IRBC-ICAM-1 catch-slip bond interactions refers to the dissociation rate at the force in which the catch-slip bond transits from catch to slip bond behavior. At 41°C, the spontaneous dissociation rate k^s of IRBC-ICAM-1 slip bond represents the dissociation rate at zero stretching force. For IRBC-CD36, whereas the spontaneous dissociation rate k^s decreased with increased temperature, the stress-free bond

TABLE 1 Fitting Parameters for Validating the Nature of IRBC-ICAM-1 Bonds at 37 and 41°C

	37°C			41°C		
Parameters	Catch-Slip	Ideal	Slip	Catch-Slip	Ideal	Slip
F ratio	627.12	335.20	379.62	244.58	84.64	1213.28
p value	7.02×10^{-8}	3.59×10^{-7}	4.82×10^{-7}	7.66×10^{-6}	3.75×10^{-5}	1.50×10^{-8}
AIC	−7.21	5.90	0.23	−6.32	9.10	−16.40
BIC	−6.42	6.06	0.47	−6.00	9.26	−16.16
R^2	0.9968	0.9795	0.9922	0.9932	0.9233	0.9975
Adjusted R^2	0.9952	0.9766	0.9895	0.9892	0.9123	0.9967

TABLE 2 Fitting Parameters for Single Bond Force-Clamp Spectroscopy and Flow Assay Obtained at Body and Febrile Temperatures

Parameter	ICAM-1		CD36	
Temperature, T (°C)	37	41	37	41
Single Bond Force-Clamp Spectroscopy				
Dissociation rate, k^x (s^{-1})	0.477	0.491	0.378	0.298
Stress-free bond length, x_0 (nm)	—	0.174	0.0866	0.400
Inverse effective spring constant, ξ ($nm \cdot pN^{-1}$)	0.00444		—	
Characteristic force, F_0 (pN)	9.70		—	
Multiple Bond Flow Assay				
Cell radius, r (μm)		3.5		
Viscosity, η (Pa·s)		0.001		
Average number of PfEMP1 proteins per single knob	3	3	2	2
Association rate, k^x_{on} (s^{-1})	0.707	0.768	1.07	0.376
Binding constant, $\frac{k^x_{on}}{k^x}$	1.48	1.56	2.83	1.26
Effective number of bonds times the width of the rupture area, $\sigma \cdot a \cdot b \cdot c$ (μm)	7.27	5.78	2.58	12.8

length x_0 at 41°C was approximately four times that at 37°C. Because x_0 is an exponential term in Eq. 4, this change reflected the more pronounced exponential decay in lifetime with increasing force (Fig. 2, *d* and *f*), indicating greater sensitivity of the bond to force. Hence, febrile temperature weakens the ability of each bond in sustaining adhesion within the mid to high force range.

The comparisons of IRBC-ICAM-1 and IRBC-CD36 single bond lifetimes at each temperature displayed less distinct differences between the interactions at physiological temperatures. At 25°C (Fig. 2, *a* and *b*), there is a clear distinction in the lifetimes of IRBC-ICAM-1 and IRBC-CD36 bonds. IRBC-CD36 single bonds survive longer at forces <5 pN and >25 pN, whereas IRBC-ICAM-1 bonds possessed longer lifetimes at forces between 12 and 17 pN. In contrast, at 37°C (Fig. 2, *c* and *d*), IRBC-CD36 single bond lifetimes are only slightly higher than IRBC-ICAM-1 at forces <5 pN, whereas the two curves largely overlap each other at forces >10 pN. The two interactions become moderately more distinguishable at 41°C (Fig. 2, *e* and *f*). The difference between IRBC-CD36 and IRBC-ICAM-1 single bond lifetimes at forces <5 pN at 41°C is larger compared to at 37°C. IRBC-ICAM-1 single bond lifetimes are also comparatively elevated between 15 and 30 pN. It is evident that temperature affects the dissociation of IRBC-receptor bonds differently at different forces. These differences may affect the synergy between ICAM-1 and CD36 in mediating cytoadhesion in vivo during the febrile cycle (50,51). Thus, for a more accurate understanding of IRBC adhesion to endothelial receptors, it is essential to perform adhesion studies at physiologically relevant temperatures.

Multiple bond flow assay at 37 and 41°C

After studying how temperature affects the dissociation of IRBC-receptor bonds, we next examined the effects on binding affinity—the ratio of its association rate to dissociation rate (52). Although the dissociation of a bond depends on properties of the limited contact region between both proteins (53), the bond association process is governed by many factors, such as the flexibility of binding proteins, chemical and geometrical environment, etc (53,54). We utilized a flow chamber assay, which provides a good platform for studying bond association by replicating the geometrical environment surroundings of the receptor-ligand pair. IRBCs were flowed over ICAM-1- or CD36-coated substrates, and the time taken for an IRBC to detach upon attachment was measured. This duration will be referred to as the cellular lifetime of the IRBC. As multiple bonds were likely to form between the IRBC and the substrate, the detachment of the cell was visualized as a chain reaction involving both the breaking of bonds (bond dissociation) as well as the rebinding of bonds (bond association). This flow assay is unlike the single bond force-clamp spectroscopy experiment whereby broken bonds did not rebind. Using dissociation rates obtained earlier as input parameters to the cellular stochastic model, we extracted the association rates for IRBC-receptor interactions at 37 and 41°C.

The multiple bond flow assay setup with temperature control is depicted in Fig. 3 *a*. Like the single bond force-clamp spectroscopy experiments, temperature of the microfluidic channel substrate was kept within ±1°C of 37 or 41°C. As demonstrated in the time lapse images in Fig. 3 *b*, the measurement of the cellular lifetime began when IRBC stopped moving and ended when the IRBC started to move along with the flow. The shear stresses used in the multiple bond flow assay were 0.014–0.042 Pa. These values are markedly lower than that in the microvasculature,

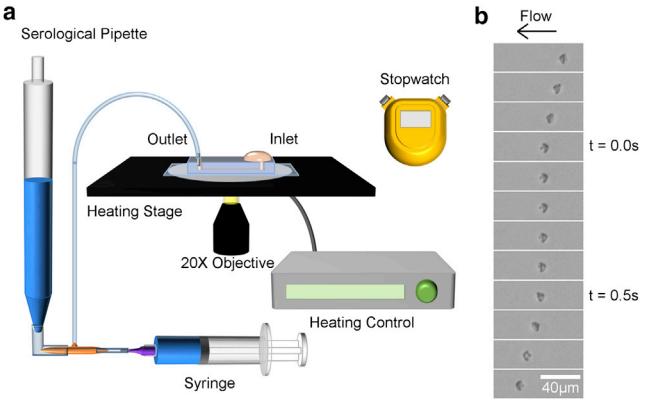

FIGURE 3 Multiple bond flow assay at physiological temperatures. (*a*) Shown is the illustration of flow assay experimental setup with the heating system. (*b*) Time lapse images of an IRBC adhering and detaching in a microfluidic channel are shown. Images were captured at time intervals of 100 ms. To see this figure in color, go online.

which ranges from 0.3 to 9.5 Pa with an average of 1.5 Pa (55). Flow assays were performed at such low shear stresses to enable the observation of IRBC attachment and detachment as well as to avoid cell rolling and adhesion bistability (39)—a phenomenon whereby IRBCs can roll at two different velocities at a given shear rate. Additionally, low densities of ICAM-1 and CD36 were functionalized on the channel substrate to keep the cellular lifetimes within reasonable limits. Higher densities of proteins would cause IRBCs to adhere for very long durations, and the experiment would be impractical to execute. Measurements were excluded when a flowing cell or cell debris contacted the attached IRBC or if the IRBC remained adhered for longer than 30 s.

The cellular lifetime versus shear stress data for both IRBC-ICAM-1 and IRBC-CD36 interactions showed a similar trend at 37°C to that obtained at 25°C (13) (Fig. 4, *a* and *b*). IRBC-ICAM-1 cellular lifetime versus shear stress curve exhibited a characteristic peak at 20 mPa, whereas IRBC-CD36 cellular lifetimes decayed with increasing shear stress. At 41°C, we observed that IRBC-CD36 cellular lifetime displayed a similar trend as at 37°C, whereas for IRBC-ICAM-1 interaction, there is a drastic change (i.e., the characteristic peak in the lifetime versus shear stress curve observed at 37°C disappeared, and the trend became similar to the IRBC-CD36 interaction) (Fig. 4, *c* and *d*). This change in trend of IRBC-ICAM-1 cellular lifetime could plausibly be due to the temperature-induced transition in the nature of single bond behavior as noted from force-clamp spectroscopy results. Moreover, for IRBC-CD36 interaction, the cellular lifetime versus shear stress curve displayed a less pronounced exponential decay as the temperature changed from 37 to 41°C (Fig. 4 *f*). This trend contradicts the observation by force-clamp spectroscopy experiments, in which the IRBC-CD36 bond lifetime has a more pronounced exponential decay as the temperature rose from 37 to 41°C (Fig. 2 *b*). A potential factor contributing to this difference is the change in association rate of IRBC-CD36 interactions with the temperature (Table 2).

Comparing both IRBC-receptor interactions at all three temperatures, our results revealed that cellular lifetimes dropped as the temperature increased from 37 to 41°C (Fig. 4, *e* and *f*)—similar to single bond lifetimes. By fitting to the model, association rates were acquired and listed in Table 1. IRBC-ICAM-1 association rate was slightly elevated at 41°C

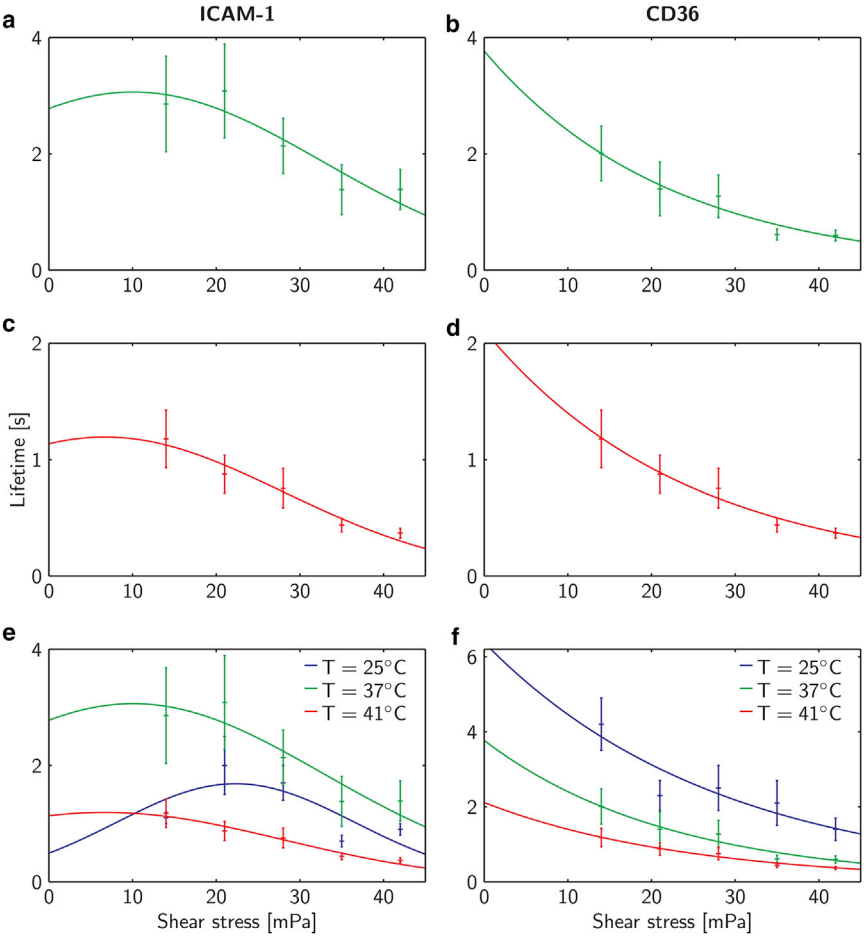

FIGURE 4 Results from multiple bond flow assay obtained at 37 and 41°C. Shown is the cellular lifetime against shear stress for IRBC-ICAM-1 and IRBC-CD36 bonds at 37°C (*a* and *b*) and 41°C (*c* and *d*). Shown is an overlay of cellular lifetime against force graphs of IRBC-ICAM-1 and IRBC-CD36 interactions at all three temperatures (*e* and *f*). Blue, green, and red are used to distinguish the experimental data and fitting obtained at 25°C (13), 37°C, and 41°C, respectively. Cellular lifetimes are plotted as mean ± SEM. To see this figure in color, go online.

(Table 2). As the dissociation rate was also elevated by a small amount, the reduced cellular lifetimes at febrile temperature could possibly be due to the greater influence of bond dissociation in affecting cellular lifetimes. In contrast, IRBC-CD36 association rate was 2.5 times lower at 41°C than at 37°C, whereas dissociation rates decreased (Table 2). The reduction in cellular lifetime at febrile temperature is hence likely to be attributed to the large reduction in the association rate. These findings support our earlier conclusion that febrile temperatures can reduce the ability of IRBCs to sustain adhesion—by increasing the tendency of bond dissociation (both ICAM-1 and CD36) as well as reducing the rate of bond formation (CD36).

The effective number of bonds formed with CD36 increased by ~4 times, whereas that with ICAM-1 remained similar as the temperature increased from 37 to 41°C (Table 2). This parameter depends on both the number of ligands on the IRBC and that on the receptors on the glass surface. IRBCs are likely to have upregulated PfEMP1 trafficking at 41°C (16), enhancing cytoadhesion by forming more bonds with endothelial receptors as seen from the CD36 data obtained. A possible reason why the same is not observed for ICAM-1 is because ICAM-1 does not adsorb as well as CD36 on glass. In our multiple bond flow assay, the concentration of ICAM-1 used to functionalize the glass substrate was 25 times that of CD36. Similarly, other flow studies also used concentrations of ICAM-1 that were 10–400 times that of CD36 (11,12). The concentration of ICAM-1 immobilized on the glass is hence likely to be lower than that of CD36. In other words, the low density of ICAM-1 immobilized on the channel restricted the number of bonds formed such that even if PfEMP1 expression had increased with the temperature, the maximum number of bonds that IRBCs can form with the substrate would not change.

Interestingly, binding affinity remained similar for IRBC-ICAM-1 but was reduced by 2.5 times for IRBC-CD36 when the temperature rose from 37 to 41°C (Table 2). Although binding affinity of IRBC-CD36 bonds was double that of IRBC-ICAM-1 bonds at normal body temperature, it was slightly lower at febrile temperature. In our earlier publication, using data collected at room temperature, we proposed that CD36 has a greater potential in mediating sequestration in brain microvasculature than commonly perceived (13). Even though endothelial CD36 is present in very low amounts in cerebral malaria patients (8), IRBC-CD36 binding affinity was 10 times that of IRBC-ICAM-1 bonds at room temperature (13). With our current results that show nonsubstantial differences in binding affinities at physiologically relevant temperatures, it seems much less likely that CD36 plays any significant role in cerebral sequestration, be it expressed on endothelium or platelets (56,57). The contrasting conclusions derived from data collected at different temperatures further emphasizes the importance of examining IRBC-receptor interactions at physiologically relevant temperatures.

DISCUSSION

Febrile cycles experienced during *P. falciparum* infection implicates that IRBC-endothelial interactions occur while the temperature in the host fluctuates between 37 and 41°C. Consequently, this work probed the effects of temperature on IRBC-receptor kinetics. Both bond dissociation models by Bell (30) and Dembo et al. (32)—which were used for fitting single bond force-clamp spectroscopy data—predicted that temperature is simply a prefactor, and other parameters are independent of it. The underlying presumption for this prediction is that the receptor-ligand bond stays the same as temperature changes (i.e., there are no structural modifications in the binding sites of either the receptor or ligand). However, our findings showed that the fitting parameters and even the nature of the bond were temperature dependent (Tables 1 and 2). This behavior suggests the occurrence of significant structural alterations with a temperature change—either in the protein or membrane structure (15)—which consequently affected single bond lifetime measurements. Thus, the importance of investigating IRBC-receptor interactions at 37 and 41°C should not be overlooked.

The significance of experimenting at physiologically relevant temperatures led us to question our current understanding of IRBC sequestration. Flow experiments conducted at room temperature have shown that CD36 facilitates static attachment, whereas ICAM-1 mediates rolling at high shear rates (11,12). These observations were supported by IRBC-receptor kinetics studied at room temperature (13). However, our results revealed that the single bond lifetimes of IRBC-ICAM-1 and IRBC-CD36 bonds were much less distinguishable at physiologically relevant temperatures. Binding affinities also changed as the temperature increased. More importantly, IRBC-ICAM-1 formed slip bonds instead of catch-slip bonds, which was believed to be the mechanism by which ICAM-1 mediates rolling (13) at 41°C. Consequently, more flow studies need to be performed at 37 and 41°C for a deeper understanding of IRBC sequestration in vivo.

Examining IRBC-receptor kinetics at physiologically relevant temperatures provided insights into adjunctive therapeutics for malaria. Febrile temperature increases and hastens the expression of PfEMP1 (16) and phosphatidylserine (17), which binds to chondroitin sulfate A, on *P. falciparum* IRBCs after exposure to febrile temperature. However, studies have suggested that febrile temperatures could also facilitate recovery from malaria by recruiting lymphocytes (58,59), inducing cytokines release (60,61), and impeding *P. falciparum* parasite growth (62). Interestingly, although phosphatidylserine upregulation increases IRBC adhesiveness, it also causes cells to be identified and phagocytosed by macrophages in the spleen (63–66). Although the World Health Organization stopped advocating the use of antipyretics in 2015 because of the risk of side effects (67), it is

still unknown if relieving fever via physical methods like sponging will be beneficial. Our biophysical study of bond kinetics at body and febrile temperatures suggests against so. Experimental data demonstrated that febrile temperature reduced the single bond lifetimes of both IRBC-receptor interactions. This result is consistent with the weakened chondroitin sulfate A-PfEMP1 bonds after exposure to febrile temperature (68). Theoretical predictions also showed that the association rate of IRBC-CD36 bonds decreased as the temperature increased. These findings suggest the potential role of fever as an approach for the body to clear sequestered IRBCs. Relief of fever could strengthen IRBC-endothelium adhesion, potentially explaining the prolonged parasite clearance time noted in some clinical trials (69,70) in which antipyretic drugs were administered.

Antiadhesion treatment is another potential way to reduce mortality caused by malaria (71). It aims to block or reverse cytoadhesion to reduce microvascular blockage (7). Soluble forms of ICAM-1 and CD36 were developed to block parasitic domains on the IRBC membrane. Although CD36 peptides were able to block the adhesion of IRBCs (72), ICAM-1 was not always successful (73). It was suggested that the catch-slip bond behavior of IRBC-ICAM-1 interactions led to the ineffectiveness of ICAM-1 peptides (13). However, we show that at 41°C, IRBC-ICAM-1 form slip bonds instead. Furthermore, the binding affinity between IRBC and CD36 is largely reduced at 41°C. We hence recommend that antiadhesion peptides should be administered during fever. This practice can potentially increase the efficiency of blocking the relevant binding sites, preventing the formation of more IRBC-receptor bonds and the rebinding of broken bonds. Furthermore, it is crucial for antiadhesion binding assays to be conducted at physiologically relevant temperatures for a better gauge of their efficacies in vivo.

Despite the valuable insights gained, it is important to acknowledge the inherent limitations of this study. IRBCs were probed while being exposed to the temperature of interest. As each experiment progresses, the duration that IRBCs were exposed to the temperature would correspondingly increase. The extent by which IRBCs remodel in response to temperature will hence change during the experiment, plausibly explaining the large scatter of data collected. Alternatively, IRBCs may first be subjected to a fix duration of heat shock before proceeding with the experiment at body temperature (17). However, it is also unknown if any remodelling of the IRBC will occur as the temperature falls back to body temperature during the experiment. We performed our experiments at the temperature of interest to better mimic the adhesion environment in vivo. Similar to Marinkovic et al. (15), we observed that late IRBCs degraded with time at 41°C, restricting the time window for conducting experiments to 3 h. Nonetheless, our work highlighted that the influence of a few degree change in temperature on binding kinetics should not be neglected in malaria as well as any biological setting.

The rationale for studying IRBC-ICAM-1 and IRBC-CD36 binding kinetics individually was to first establish a fundamental understanding of these interactions. Moving forward, future studies are necessary to determine the exact in vivo flow conditions or locations in the body when and where the catch-slip transition is important. Our results show that the catch-slip transition occurs at low stress flows (~0.01 Pa), whereby the force acting per bond is low. Although physiological shear stress values in the microvasculature are typically above 0.1 Pa, the shear stress in vivo can be heterogeneous, and the smallest shear stress in the human body could be on the order of 0.01 Pa (55,74). It is noteworthy that, from the perspective of single bond characteristics, it is more relevant to account for the actual force acting on each bond instead of the shear stress acting on the entire IRBC. However, it is not yet known how many bonds are formed exactly between the IRBCs and ICAM-1 on the endothelial cells in vivo. Further investigations on exact flow conditions in vivo would enhance our understanding of the physiological relevance of the catch-slip transition observed in our work.

Additionally, future efforts should concentrate on studying the synergy of ICAM-1 and CD36 in mediating cytoadhesion. Existing literature on this synergy were of adhesion assays performed either under static conditions at 37°C or under flow at room temperature (12,50). Investigating the synergy of these receptors under flow conditions—because of the IRBC-ICAM-1 catch-slip bond behavior (13)—at physiologically relevant temperatures will thus provide a more accurate depiction of what occurs in vivo and contribute greatly to the development of therapeutics.

SUPPORTING MATERIAL

Supporting Material can be found online at https://doi.org/10.1016/j.bpj.2019.11.016.

AUTHOR CONTRIBUTIONS

Y.B.L., J.T., F.K., M.D., J.C., and C.T.L. conceived and designed the experiments. Y.B.L. performed the experiments. F.K. designed the force spectroscopy heating system. J.T. performed the theoretical modeling. Y.B.L., J.T., and F.K. analyzed the results. All authors reviewed the manuscript.

ACKNOWLEDGMENTS

The authors are grateful to Prof. Hans-Peter Beck's group for developing the *MAHRP1* knockout strain as well as Prof. Peter Preiser for sharing it. They also deeply appreciate the facilities provided by Global Enterprise for Micro-Mechanics and Molecular Medicine and Singapore-Massachusetts Institute of Technology Alliance for Research and Technology Infectious Diseases Interdisciplinary Research Group.

C.T.L. acknowledges support from the Institute for Health Innovation and Technology (iHealthtech) at the National University of Singapore. Y.B.L. is funded by the SMA Graduate Fellowship at Singapore-Massachusetts Institute of Technology Alliance for Research and Technology. J.T.

acknowledges the support by the Institute for Basic Science in Korea (IBS-R024-Y2).

REFERENCES

1. World Health Organisation. 2017. World Malaria Report 2017.
2. Miller, L. H., D. I. Baruch, …, O. K. Doumbo. 2002. The pathogenic basis of malaria. *Nature.* 415:673–679.
3. Dondorp, A. M., S. J. Lee, …, N. J. White. 2008. The relationship between age and the manifestations of and mortality associated with severe malaria. *Clin. Infect. Dis.* 47:151–157.
4. Marsh, K., D. Forster, …, R. Snow. 1995. Indicators of life-threatening malaria in African children. *N. Engl. J. Med.* 332:1399–1404.
5. Mebius, R. E., and G. Kraal. 2005. Structure and function of the spleen. *Nat. Rev. Immunol.* 5:606–616.
6. Chen, Q., M. Schlichtherle, and M. Wahlgren. 2000. Molecular aspects of severe malaria. *Clin. Microbiol. Rev.* 13:439–450.
7. Rowe, J. A., A. Claessens, …, M. Arman. 2009. Adhesion of Plasmodium falciparum-infected erythrocytes to human cells: molecular mechanisms and therapeutic implications. *Expert Rev. Mol. Med.* 11:e16.
8. Turner, G. D., H. Morrison, …, B. Nagachinta. 1994. An immunohistochemical study of the pathology of fatal malaria. Evidence for widespread endothelial activation and a potential role for intercellular adhesion molecule-1 in cerebral sequestration. *Am. J. Pathol.* 145:1057–1069.
9. Tuikue Ndam, N., A. Moussiliou, …, P. Deloron. 2017. Parasites causing cerebral falciparum malaria bind multiple endothelial receptors and express EPCR and ICAM-1-binding PfEMP1. *J. Infect. Dis.* 215:1918–1925.
10. Craig, A. G., M. F. Khairul, and P. R. Patil. 2012. Cytoadherence and severe malaria. *Malays. J. Med. Sci.* 19:5–18.
11. Cooke, B. M., A. R. Berendt, …, G. B. Nash. 1994. Rolling and stationary cytoadhesion of red blood cells parasitized by Plasmodium falciparum: separate roles for ICAM-1, CD36 and thrombospondin. *Br. J. Haematol.* 87:162–170.
12. Gray, C., C. McCormick, …, A. Craig. 2003. ICAM-1 can play a major role in mediating P. falciparum adhesion to endothelium under flow. *Mol. Biochem. Parasitol.* 128:187–193.
13. Lim, Y. B., J. Thingna, …, C. T. Lim. 2017. Single molecule and multiple bond characterization of catch bond associated cytoadhesion in malaria. *Sci. Rep.* 7:4208.
14. Crutcher, J. M., and S. L. Hoffman. 1996. Malaria. *In* Medical Microbiology. S. Baron, ed. University of Texas Medical Branch at Galveston.
15. Marinkovic, M., M. Diez-Silva, …, J. P. Butler. 2009. Febrile temperature leads to significant stiffening of Plasmodium falciparum parasitized erythrocytes. *Am. J. Physiol. Cell Physiol.* 296:C59–C64.
16. Udomsangpetch, R., B. Pipitaporn, …, N. J. White. 2002. Febrile temperatures induce cytoadherence of ring-stage Plasmodium falciparum-infected erythrocytes. *Proc. Natl. Acad. Sci. USA.* 99:11825–11829.
17. Zhang, R., R. Chandramohanadas, …, M. Dao. 2018. Febrile temperature elevates the expression of phosphatidylserine on Plasmodium falciparum (FCR3CSA) infected red blood cell surface leading to increased cytoadhesion. *Sci. Rep.* 8:15022.
18. Johnstone, R. W., S. M. Andrew, …, I. F. McKenzie. 1990. The effect of temperature on the binding kinetics and equilibrium constants of monoclonal antibodies to cell surface antigens. *Mol. Immunol.* 27:327–333.
19. Lipschultz, C. A., A. Yee, …, S. J. Smith-Gill. 2002. Temperature differentially affects encounter and docking thermodynamics of antibody–antigen association. *J. Mol. Recognit.* 15:44–52.
20. Frauenfelder, H., G. A. Petsko, and D. Tsernoglou. 1979. Temperature-dependent X-ray diffraction as a probe of protein structural dynamics. *Nature.* 280:558–563.
21. Tilton, R. F., Jr., J. C. Dewan, and G. A. Petsko. 1992. Effects of temperature on protein structure and dynamics: X-ray crystallographic studies of the protein ribonuclease-A at nine different temperatures from 98 to 320 K. *Biochemistry.* 31:2469–2481.
22. Li, A., T. S. Lim, …, C. T. Lim. 2011. Molecular mechanistic insights into the endothelial receptor mediated cytoadherence of Plasmodium falciparum-infected erythrocytes. *PLoS One.* 6:e16929.
23. University of Edinburgh. 2007. Culturing Plasmodium falciparum (Standard Operating Procedure).
24. Ribaut, C., A. Berry, …, A. Valentin. 2008. Concentration and purification by magnetic separation of the erythrocytic stages of all human Plasmodium species. *Malar. J.* 7:45.
25. Liu, F., J. Burgess, …, A. Ostafin. 2003. Sample preparation and imaging of erythrocyte cytoskeleton with the atomic force microscopy. *Cell Biochem. Biophys.* 38:251–270.
26. Johnson, K. C., and W. E. Thomas. 2018. How do we know when single-molecule force spectroscopy really tests single bonds? *Biophys. J.* 114:2032–2039.
27. Shao, J. Y., and G. Xu. 2007. The adhesion between a microvillus-bearing cell and a ligand-coated substrate: a Monte Carlo study. *Ann. Biomed. Eng.* 35:397–407.
28. Piper, J. W., R. A. Swerlick, and C. Zhu. 1998. Determining force dependence of two-dimensional receptor-ligand binding affinity by centrifugation. *Biophys. J.* 74:492–513.
29. Evans, E. 2001. Probing the relation between force–lifetime–and chemistry in single molecular bonds. *Annu. Rev. Biophys. Biomol. Struct.* 30:105–128.
30. Bell, G. I. 1978. Models for the specific adhesion of cells to cells. *Science.* 200:618–627.
31. Evans, E., and K. Ritchie. 1997. Dynamic strength of molecular adhesion bonds. *Biophys. J.* 72:1541–1555.
32. Dembo, M., D. C. Torney, …, D. Hammer. 1988. The reaction-limited kinetics of membrane-to-surface adhesion and detachment. *Proc. R. Soc. Lond. B Biol. Sci.* 234:55–83.
33. Zhu, C., J. Lou, and R. P. McEver. 2005. Catch bonds: physical models, structural bases, biological function and rheological relevance. *Biorheology.* 42:443–462.
34. Chakrabarti, S., M. Hinczewski, and D. Thirumalai. 2017. Phenomenological and microscopic theories for catch bonds. *J. Struct. Biol.* 197:50–56.
35. Pereverzev, Y. V., O. V. Prezhdo, …, W. E. Thomas. 2005. The two-pathway model for the catch-slip transition in biological adhesion. *Biophys. J.* 89:1446–1454.
36. Yuan, G., S. Le, …, H. Chen. 2017. Elasticity of the transition state leading to an unexpected mechanical stabilization of titin immunoglobulin domains. *Angew. Chem. Int.Engl.* 56:5490–5493.
37. Guo, S., Q. Tang, …, J. Yan. 2018. Structural-elastic determination of the force-dependent transition rate of biomolecules. *Chem. Sci. (Camb.).* 9:5871–5882.
38. Xu, X., A. K. Efremov, …, J. Cao. 2013. Probing the cytoadherence of malaria infected red blood cells under flow. *PLoS One.* 8:e64763.
39. Efremov, A., and J. Cao. 2011. Bistability of cell adhesion in shear flow. *Biophys. J.* 101:1032–1040.
40. Hammer, D. A., and D. A. Lauffenburger. 1987. A dynamical model for receptor-mediated cell adhesion to surfaces. *Biophys. J.* 52:475–487.
41. Erdmann, T., and U. S. Schwarz. 2004. Stability of adhesion clusters under constant force. *Phys. Rev. Lett.* 92:108102.
42. Erdmann, T., and U. S. Schwarz. 2004. Stochastic dynamics of adhesion clusters under shared constant force and with rebinding. *J. Chem. Phys.* 121:8997–9017.
43. Bar-Haim, A., and J. Klafter. 1998. On mean residence and first passage times in finite one-dimensional systems. *J. Chem. Phys.* 109:5187–5193.

44. Cao, J., and R. J. Silbey. 2008. Generic schemes for single-molecule kinetics. 1: self-consistent pathway solutions for renewal processes. *J. Phys. Chem. B.* 112:12867–12880.

45. Marshall, B. T., M. Long, …, C. Zhu. 2003. Direct observation of catch bonds involving cell-adhesion molecules. *Nature.* 423:190–193.

46. Sarangapani, K. K., T. Yago, …, C. Zhu. 2004. Low force decelerates L-selectin dissociation from P-selectin glycoprotein ligand-1 and endoglycan. *J. Biol. Chem.* 279:2291–2298.

47. Rakshit, S., Y. Zhang, …, S. Sivasankar. 2012. Ideal, catch, and slip bonds in cadherin adhesion. *Proc. Natl. Acad. Sci. USA.* 109:18815–18820.

48. Burnham, K. P., and D. R. Anderson. 2003. Model Selection and Multimodel Inference. Springer, New York.

49. Schumakovitch, I., W. Grange, …, M. Hegner. 2002. Temperature dependence of unbinding forces between complementary DNA strands. *Biophys. J.* 82:517–521.

50. McCormick, C. J., A. Craig, …, A. R. Berendt. 1997. Intercellular adhesion molecule-1 and CD36 synergize to mediate adherence of Plasmodium falciparum-infected erythrocytes to cultured human microvascular endothelial cells. *J. Clin. Invest.* 100:2521–2529.

51. Yipp, B. G., S. Anand, …, M. Ho. 2000. Synergism of multiple adhesion molecules in mediating cytoadherence of Plasmodium falciparum-infected erythrocytes to microvascular endothelial cells under flow. *Blood.* 96:2292–2298.

52. Du, X., Y. Li, …, S. Q. Liu. 2016. Insights into protein-ligand interactions: mechanisms, models, and methods. *Int. J. Mol. Sci.* 17:E144.

53. Pierres, A., A. M. Benoliel, and P. Bongrand. 1998. Studying receptor-mediated cell adhesion at the single molecule level. *Cell Adhes. Commun.* 5:375–395.

54. Bongrand, P. 1999. Ligand-receptor interactions. *Rep. Prog. Phys.* 62:921–968.

55. Koutsiaris, A. G., S. V. Tachmitzi, …, D. Z. Chatzoulis. 2007. Volume flow and wall shear stress quantification in the human conjunctival capillaries and post-capillary venules in vivo. *Biorheology.* 44:375–386.

56. Grau, G. E., C. D. Mackenzie, …, M. E. Molyneux. 2003. Platelet accumulation in brain microvessels in fatal pediatric cerebral malaria. *J. Infect. Dis.* 187:461–466.

57. Wassmer, S. C., C. Lépolard, …, G. E. Grau. 2004. Platelets reorient Plasmodium falciparum-infected erythrocyte cytoadhesion to activated endothelial cells. *J. Infect. Dis.* 189:180–189.

58. Chen, Q., D. T. Fisher, …, S. S. Evans. 2006. Fever-range thermal stress promotes lymphocyte trafficking across high endothelial venules via an interleukin 6 trans-signaling mechanism. *Nat. Immunol.* 7:1299–1308.

59. Chen, Q., M. M. Appenheimer, …, S. S. Evans. 2009. Thermal facilitation of lymphocyte trafficking involves temporal induction of intravascular ICAM-1. *Microcirculation.* 16:143–158.

60. Dodoo, D., F. M. Omer, …, E. M. Riley. 2002. Absolute levels and ratios of proinflammatory and anti-inflammatory cytokine production in vitro predict clinical immunity to Plasmodium falciparum malaria. *J. Infect. Dis.* 185:971–979.

61. Mordmüller, B. G., W. G. Metzger, …, P. G. Kremsner. 1997. Tumor necrosis factor in Plasmodium falciparum malaria: high plasma level is associated with fever, but high production capacity is associated with rapid fever clearance. *Eur. Cytokine Netw.* 8:29–35.

62. Long, H. Y., B. Lell, …, P. G. Kremsner. 2001. Plasmodium falciparum: in vitro growth inhibition by febrile temperatures. *Parasitol. Res.* 87:553–555.

63. Lang, P. A., R. S. Kasinathan, …, S. M. Huber. 2009. Accelerated clearance of Plasmodium-infected erythrocytes in sickle cell trait and annexin-A7 deficiency. *Cell. Physiol. Biochem.* 24:415–428.

64. Schroit, A. J., J. W. Madsen, and Y. Tanaka. 1985. In vivo recognition and clearance of red blood cells containing phosphatidylserine in their plasma membranes. *J. Biol. Chem.* 260:5131–5138.

65. Turrini, F., H. Ginsburg, …, P. Arese. 1992. Phagocytosis of Plasmodium falciparum-infected human red blood cells by human monocytes: involvement of immune and nonimmune determinants and dependence on parasite developmental stage. *Blood.* 80:801–808.

66. Tanaka, Y., and A. J. Schroit. 1983. Insertion of fluorescent phosphatidylserine into the plasma membrane of red blood cells. Recognition by autologous macrophages. *J. Biol. Chem.* 258:11335–11343.

67. World Health Organisation. 2015. Use of Antipyretics, Third Edition. World Health Organization, Geneva.

68. Carvalho, P. A., M. Diez-Silva, …, S. Suresh. 2013. Cytoadherence of erythrocytes invaded by Plasmodium falciparum: quantitative contact-probing of a human malaria receptor. *Acta Biomater.* 9:6349–6359.

69. Meremikwu, M., K. Logan, and P. Garner. 2000. Antipyretic measures for treating fever in malaria. *Cochrane Database Syst. Rev.* 200:CD002151.

70. Brandts, C. H., M. Ndjavé, …, P. G. Kremsner. 1997. Effect of paracetamol on parasite clearance time in Plasmodium falciparum malaria. *Lancet.* 350:704–709.

71. Simmons, D. L. 2005. Anti-adhesion therapies. *Curr. Opin. Pharmacol.* 5:398–404.

72. Baruch, D. I., X. C. Ma, …, L. H. Miller. 1999. CD36 peptides that block cytoadherence define the CD36 binding region for Plasmodium falciparum-infected erythrocytes. *Blood.* 94:2121–2127.

73. Craig, A. G., R. Pinches, …, A. R. Berendt. 1997. Failure to block adhesion of Plasmodium falciparum-infected erythrocytes to ICAM-1 with soluble ICAM-1. *Infect. Immun.* 65:4580–4585.

74. Papaioannou, T. G., and C. Stefanadis. 2005. Vascular wall shear stress: basic principles and methods. *Hellenic J. Cardiol.* 46:9–15.

Biophysical Journal, Volume *118*

Supplemental Information

Temperature-Induced Catch-Slip to Slip Bond Transit in *Plasmodium falciparum*-Infected Erythrocytes

Ying Bena Lim, Juzar Thingna, Fang Kong, Ming Dao, Jianshu Cao, and Chwee Teck Lim

Supporting Information 1. Validation of AFM tip functionalization protocol

To validate the AFM tip functionalization protocol, antibodies conjugated with dyes were used to detect the presence of the receptors. AFM tips were prepared in four different ways: 1) Untreated; 2) Functionalized with PEG linker followed by deactivation of excess amine groups with glycine; 3) Functionalized with 100µg/ml ICAM-1; 4) Functionalized with 100µg/ml CD36. The first two AFM tips acted as negative controls for determining the background noise in the imaging. All tips were incubated in the dark for 30min in a fluorescence dye solution comprising 0.3µl of 200µg/ml Phycoerythrin (PE) anti-human CD54 (also known as ICAM-1) (BioLegend) and 0.3µl of 300µg/ml Fluorescein (FITC) anti-human CD36 (BioLegend) in 50µl 1×PBS. Thereafter, the tips were washed in 1×PBS before imaging under the microscope. Images captured were processed using ImageJ (NIH) to eliminate background noise. This process was executed for each excitation wavelength by normalizing to the image of the bare AFM tip in that viewing mode. All images taken under the same excitation wavelength were handled using the same method to prevent misrepresentation of the staining outcome.

As presented in Fig. S1, there were clear positive fluorescence signals for both ICAM-1 and CD36 functionalized tips. The AFM tip functionalization protocol was hence proven to be successful.

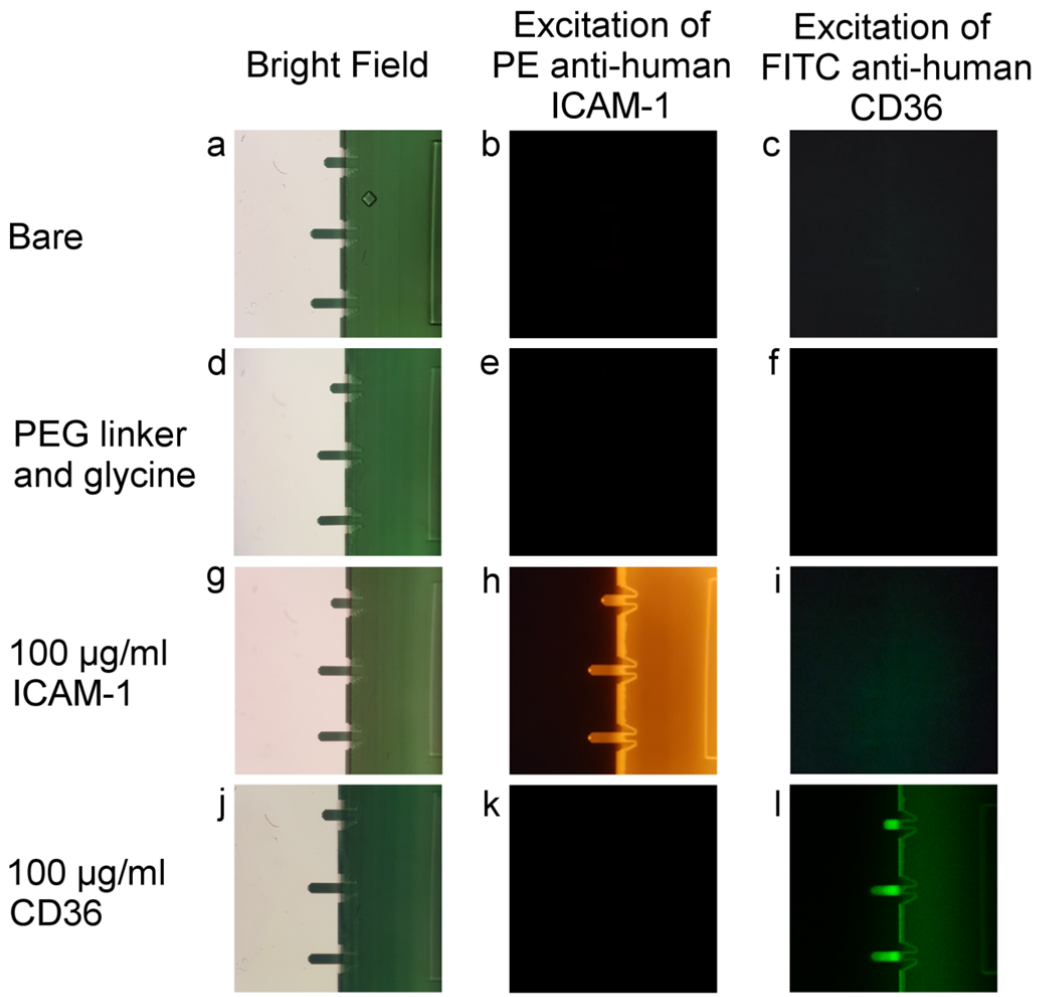

Figure S1. Validation of AFM tip functionalization protocol. (a-c) Bare tip imaged under bright field, excitation wavelength of PE dye and excitation wavelength of FITC dye, respectively. (d-f) Tip functionalized with PEG linkers imaged under bright field, excitation wavelength of PE dye and excitation wavelength of FITC dye, respectively. (g-i) Tip functionalized with ICAM-1 imaged under bright field, excitation wavelength of PE dye and excitation wavelength of FITC dye, respectively. (j-l) Tip functionalized with CD36 imaged under bright field, excitation wavelength of PE dye and excitation wavelength of FITC dye, respectively.

Supplementary Information 2. Force Spectroscopy heating system

The circuitry of the heating system used to regulate the temperature of the heating element is illustrated in Fig. S2 (a). The temperature of the heating element was monitored by using the type k thermocouple. This information served as a feedback to the proportional-integral-derivative (PID) controller (XMTG-700W, Yuyao Yutai Meter Co., Ltd.). The PID controller was responsible for controlling the solid state relay (SSR) (Delixi Electric) which was a switch for the live wire. When the temperature was beneath the set temperature, the controller delivered a small voltage to the SSR, thereby closing the switch for the live wire. The transformer and rectifier then converted the 220V alternating current (AC) supply to 5V direct current (DC). This 5V potential difference subsequently caused the heating element to heat up. Once the temperature reached the set temperature, the switch for the live wire was opened and the heating ended. The auto tune function of the PID controller was employed to optimize its response to the temperature of the heating element for enhanced temperature stability throughout the experiment.

This heating system was integrated with the AFM set-up as shown in Fig. S2 (b). As the entire set-up is an open system, there will be heat loss from the substrate to the surrounding laboratory environment and the temperature of the heating element will not reflect that of the substrate. Fig. S2 (c) shows the thermocouple of the thermometer in direct contact with the substrate to facilitate the monitoring of substrate temperature throughout the experiment. The temperature of the substrate was kept within ± 1°C of the set temperature – 37°C and 41°C.

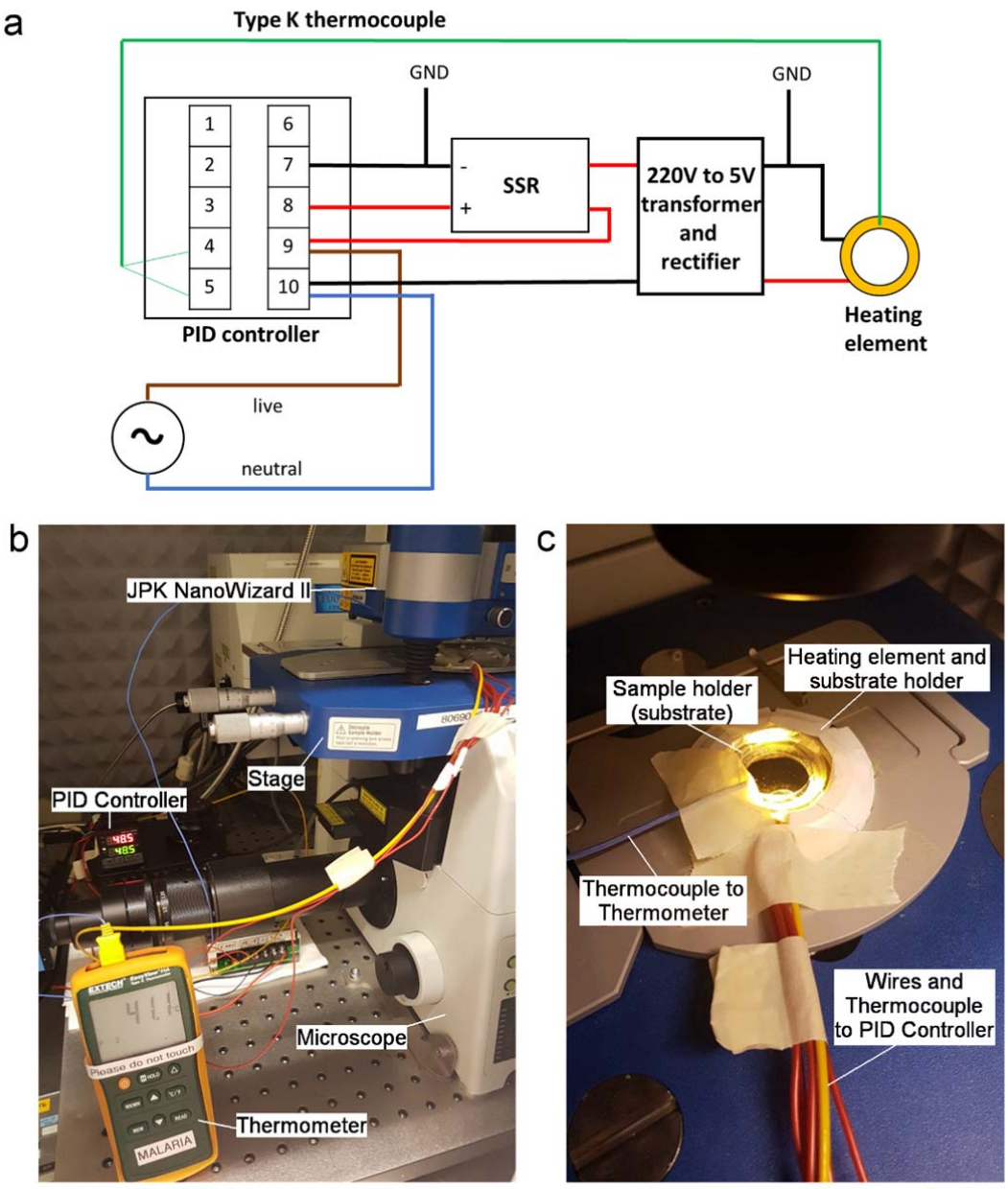

Figure S2. Heating system for single bond force spectroscopy. (a) Circuitry (b) Experimental set-up with heating system. (c) Set-up on the microscope stage.

Supporting Information 3. Validation of microfluidic channel functionalization protocol

The microfluidic channel functionalization protocol was also verified by using antibodies conjugated with dyes. Microfluidic channels were prepared in three ways: 1) Incubated with only 5% BSA in 1×PBS; 2) Functionalized 100µg/ml ICAM-1; 3) Functionalized with 100µg/ml CD36. The first channel served as a negative control for setting the baseline of the background noise in the captured images. All channels were infused with a fluorescence dye solution comprising 0.3µl of 200µg/ml PE anti-human CD54 and 0.3µl of 300µg/ml FITC anti-human CD36 in 50µl 1×PBS. After 30min incubation in the dark, the channels were rinsed with 1×PBS. Images of the channels were subsequently captured using a camera mounted on the microscope. Lastly, ImageJ (NIH) was used to extract the background noise from each image by normalizing to the image of the channel incubated with just 5% BSA. All images captured under the same excitation wavelength were handled in the same manner to avoid misrepresenting the staining results.

Fig. S3 showed distinct fluorescence signals for both ICAM-1 and CD36 functionalized microfluidic channels. The microfluidic channel functionalization protocol was thus ascertained to be successful.

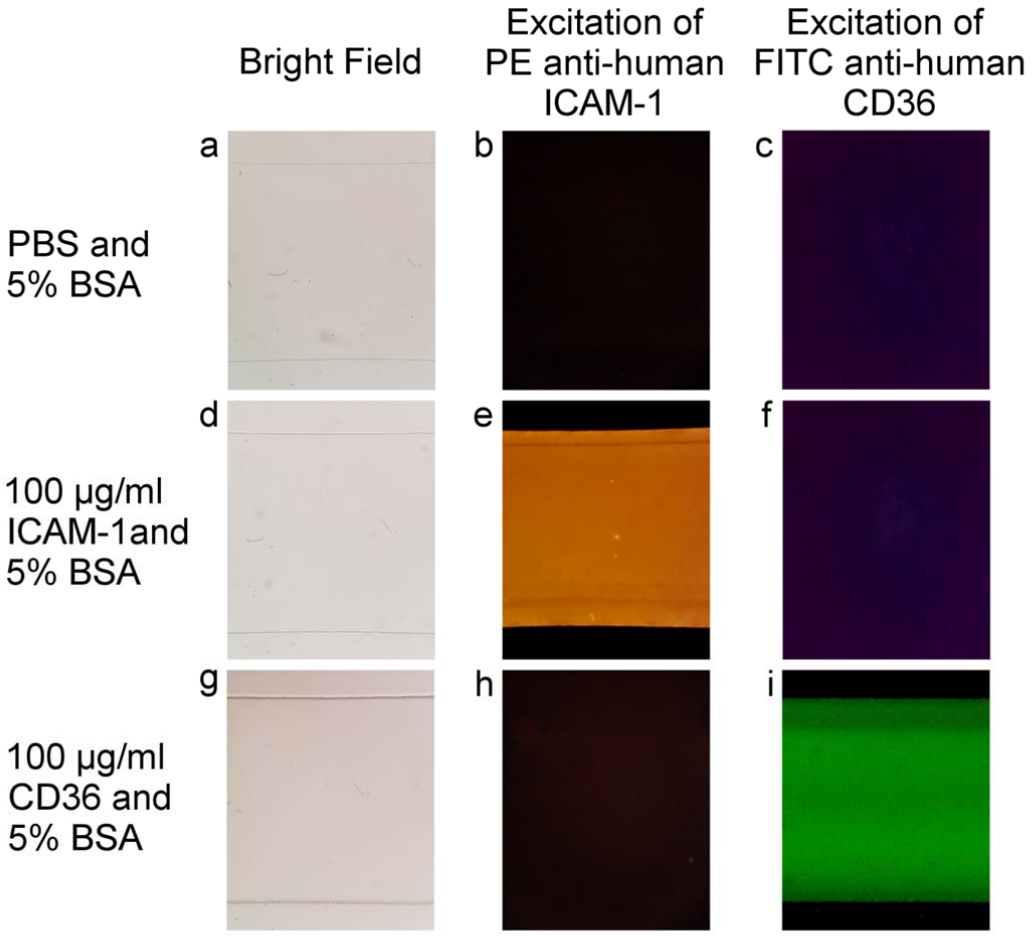

Figure S3. Validation of microfluidic channel functionalization protocol. (a-c) Microfluidic channel blocked with 5% BSA captured under bright field, excitation wavelength of PE dye and excitation wavelength of FITC dye, respectively. (d-f) Microfluidic channel functionalized with ICAM-1 captured under bright field, excitation wavelength of PE dye and excitation wavelength of FITC dye, respectively. (g-i) Microfluidic channel functionalized with CD36 captured under bright field, excitation wavelength of PE dye and excitation wavelength of FITC dye, respectively.

Supporting Information 4. Microfluidic flow assay heating system

Microfluidic flow assays used to study multiple bond adhesion were also conducted at physiologically relevant temperatures. For temperature control, a heating stage (Linkam Scientific, DC60) was fitted onto the microscope stage (Fig. S4 (a)). To directly monitor the temperature of the substrate, the thermocouple of the thermometer was placed in contact with the microfluidic channel substrate at the reservoir inlet (Fig. S4 (b)). The temperature of the microfluidic channel substrate was kept within ± 1°C of body or febrile temperature.

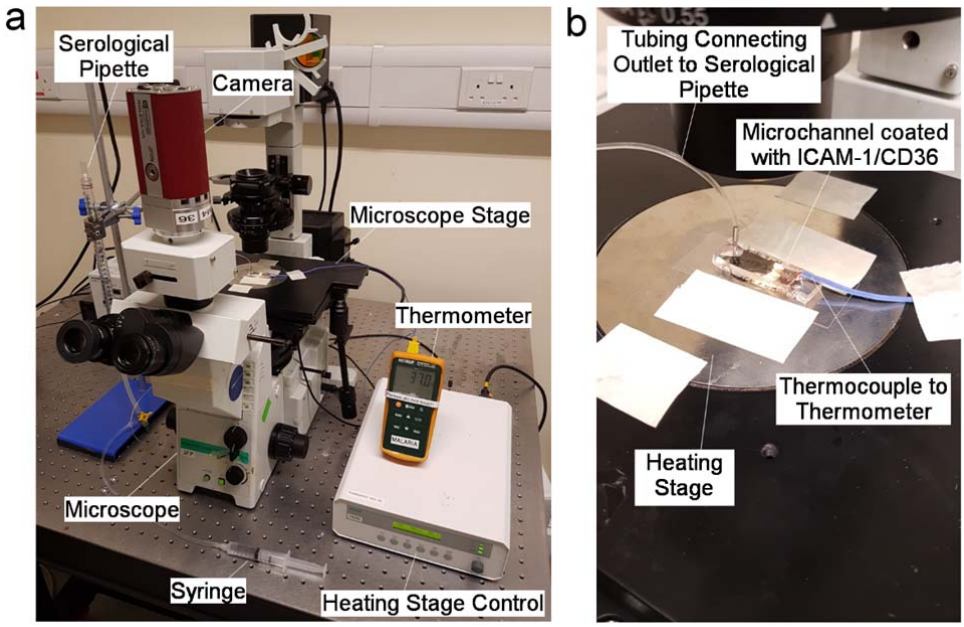

Figure S4. Heating system for multiple bond flow assay. (a) Experimental set-up with heating system. (b) Set-up on the microscope stage.

Supporting Information 5. Microfluidic flow calculations

Several equations were used to aid in correlating the pressure difference between the inlet and outlet to the shear stress within the channel. First, the pressure difference ΔP due to a change in height of the water level in the serological pipette ΔH is:

$$\Delta P = \rho g \Delta H \qquad \text{(S5.1)}$$

where ρ is the density of water while g is the acceleration due to gravity. The volumetric flow rate Q_v in the channel as a result of ΔP is:

$$Q_v = \frac{\Delta P w h^3}{a_h \mu L}. \qquad \text{(S5.2)}$$

Here, w is the channel width, h is the channel height , L is the channel length and μ is the viscosity of malaria culture medium(1). The geometric factor due to hydraulic resistance in rectangular channels $a_h = 12\left[1 - \frac{192h}{\pi^5 w}\tanh\left(\frac{\pi w}{2h}\right)\right]^{-1}$ (1). Finally, the wall shear stress in a rectangular channel

$$\tau_w = \frac{6\mu Q_v}{w h^2} \text{ (2).} \qquad \text{(S5.3)}$$

By combining Eqs. S6.1, S6.2 and S6.3, we obtain the expression

$$\tau_w = \frac{6\rho g \Delta H h}{a_h L}. \qquad \text{(S5.4)}$$

A volume change of 10ml in the serological pipette used in our set-up corresponds to a change in the water level by 8cm**.** Resultantly, by using Eq. S5.4, a 0.2ml change in volume within the serological pipette will lead to a 0.014 Pa change in wall shear stress τ_w.

The type of flow in the microfluidic channel was determined by calculating the Reynolds number Re using

$$\mathrm{Re} = \frac{\rho U D_h}{\mu} \text{ (3).} \qquad \text{(S5.5)}$$

In this equation, the average flow velocity $U = \frac{Q_v}{wh}$ and the hydraulic diameter $D_h = \frac{2wh}{w+h}$. A laminar flow is one where $\mathrm{Re} < 2300$. Since $\mathrm{Re} = 0.0128$ for the highest shear rate used in our flow assays, the nature of the flow in all our experiments were laminar. The entry length L_e is the distance in the microfluidic channel from the inlet for the flow to be fully developed. It can be determined using

$$L_e \cong 0.085\,\mathrm{Re}\,D_h \text{ (3).} \qquad \text{(S5.6)}$$

Calculations reveal that $L_e = 5.68 \times 10^{-8} m$ for the highest shear rate used. Hence, the laminar flow will be fully developed at the middle of the channel - 0.75cm from the inlet - where the field of view is set.

Supporting Information 6. Adhesion specificity of ICAM-1 and CD36 to PfEMP1

P. falciparum IRBCs can interact with host cells via parasite-exported proteins localized on knobs (4, 5) - electron-dense protruding structures of the host RBC membrane (6, 7). The known IRBC ligands include *P. falciparum* Erythrocyte Membrane Protein-1 (PfEMP1) encoded by *var* genes (8), STEVOR encoded by subtelomeric variant open reading frame (*stevor*) (9, 10) and RIFIN (11) encoded by repetitive interspersed family (*rif)*. PfEMP1 is regulated by approximately 60 *var* genes per parasite genome (8). This IRBC ligand has been shown to bind to host cell receptors such as ICAM-1 and CD36 (12). Another study observed that fever-induced cytoadherence is attributed by the increased trafficking of PfEMP1 to the IRBC membrane (13). Even though the functions of RIFIN and STEVOR are not as well explored as PfEMP1, they might also interact with ICAM-1.

A 3D7 mutant with a disruption in the membrane-associated histidine-rich protein 1 (MAHRP1) gene was used to determine the adhesion specificity of the endothelial receptors to PfEMP1. MAHRP1 is a transmembrane protein that is expressed during ring stages of the parasite (14). It remains available during the entire IRBC life cycle, and is exported beyond the parasite's vacuole into parasite-derived membrane-bound structures known as Maurer's clefts (6)- intermediate trafficking chambers for proteins that are supposed to be expressed on the IRBC membrane (15). Spycher et al. (15) generated a deletion mutant of the *MAHRP1* gene and discovered that PfEMP1 could not be detected on the host membrane. Instead, PfEMP1 simply accumulates within the parasitic vacuole.

The adhesion specificity to PfEMP1 was determined by studying various interactions: 1) Late IRBCs probed with tip functionalized with just the PEG-linkers; 2) Uninfected RBCs probed with tip functionalized with receptor; 3) Late *MAHRP1* KO IRBCs probed with tip functionalized with receptor and 4) Late IRBCs probed with tip functionalized with receptor.

All experiments were performed at room, body and febrile temperatures using the same concentrations and parameters for condition 4.

The raw data collected were categorized based on whether any breaking events were observed. The total number of curves with breaking events before, during or after the 10s force clamp was classified as the total number of adhesion curves. This group was then further split into curves with a measurable lifetime - only one breaking event during the 10s force clamp period - or curves that did not. The number of curves with one measurable lifetime was labelled as the number of single bond lifetimes. For each experimental condition, the percentage of the number of single bond lifetimes against total number of adhesion curves was computed. After processing the data from all conditions, the values were collated in Table S6.

Table S6. Percentage of number of single bond lifetimes against the total number of adhesion curves.

T (°C)	**Percentage of number of single bond lifetimes / total number of adhesion curves**						
	Tip Control	**Tip functionalized with ICAM-1**			**Tip functionalized with CD36**		
	PEG linker + Glycine	RBC	*MAHRP1* KO IRBCs	IRBC	RBC	*MAHRP1* KO IRBCs	IRBC
25	7.5	9.6	8.2	42.7	0.0	8.7	31.3
37	0.8	4.0	2.3	14.2	5.0	0.7	13.5
41	2.0	1.7	2.1	11.4	1.3	3.6	16.4

The percentage of number of single bond lifetimes against the total number of adhesion curves for each condition reflects the efficiency of the interaction in attaining a measurable single bond lifetime value at any force. By comparing the efficiencies across different conditions, it was possible to estimate the percentage of non-specific adhesions arising from various sources.

The efficiency of obtaining single bond lifetimes with ICAM-1-functionalized AFM tip was about four times higher for IRBCs as compared to *MAHRP1* KO IRBCs at all three temperatures. In other words, the specificity of PfEMP1-ICAM-1 interactions was roughly 80%. Considering that the efficiency was similar for ICAM-1-RBC and ICAM-1-*MAHRP1* KO IRBCs interactions, it is unlikely that ICAM-1 binds to IRBC ligands other than PfEMP1. In the case of the CD36-functionalized tip, the efficiency for obtaining single bond lifetimes was approximately three times higher for IRBCs as compared to *MAHRP1* KO IRBCs. The specificity of PfEMP1-CD36 interactions was thus estimated to be 75%. Since the efficiency also seemed to be comparable for both CD36-*MAHRP1* KO IRBCs and CD36-RBC adhesion, it is unlikely that CD36 may have also bound to other IRBC ligands during the force-clamp spectroscopy experiments. Indeed, studies have reported that RIFINs are not detected on the 3D7 strain(16) - which is used in this investigation - and STEVOR does not bind to CD36(17).

Bearing in mind that the efficiency of observing single bond lifetimes was similar for both RBC-receptor and *MAHRP1* KO IRBC-receptor interactions, the main source of non-specific adhesions is likely to be the RBC membrane. It was also observed that there was a higher proportion of breaking events occurring before and after the 10s force clamp period for all interactions at 37°C and 41°C. Consequently, the efficiency of obtaining single bond lifetimes was lowered across all conditions. This phenomenon could be attributed to the different force spectroscopy parameters and functionalization concentrations from that of 25°C (18). Nonetheless, the specificity of PfEMP1-receptor interactions remains relatively similar at all temperatures at approximately 80%.

References

1. Das, P.K., H.P. Gunterman, A. Kwong, and A. Weber Z. 2013. Liquid-Water Uptake and Removal in PEM Fuel-Cell Components. .

2. Bird, R.B., W.E. Stewart, and E.N. Lightfoot. 1960. Transport phenomena. New York, NY: John Wiley and Sons, Inc.

3. Kleinstreuer, C. 2010. Modern Fluid Dynamics. Dordrecht: Springer Netherlands.

4. van Schravendijk, M.R., E.P. Rock, K. Marsh, Y. Ito, M. Aikawa, J. Neequaye, D. Ofori-Adjei, R. Rodriguez, M.E. Patarroyo, and R.J. Howard. 1991. Characterization and localization of Plasmodium falciparum surface antigens on infected erythrocytes from west African patients. Blood. 78: 226–36.

5. Nakamura, K., T. Hasler, K. Morehead, R.J. Howard, and M. Aikawa. 1992. Plasmodium falciparum-infected erythrocyte receptor(s) for CD36 and thrombospondin are restricted to knobs on the erythrocyte surface. J. Histochem. Cytochem. 40: 1419–22.

6. Aikawa, M., and L.H. Miller. 2008. Structural Alteration of the Erythrocyte Membrane During Malarial Parasite Invasion and Intraerythrocytic Development. In: Evered D, J Whelan, editors. Malaria and the Red Cell. . pp. 45–63.

7. Gruenberg, J., D.R. Allred, and I.W. Sherman. 1983. Scanning electron microscope-analysis of the protrusions (knobs) present on the surface of Plasmodium falciparum-infected erythrocytes. J. Cell Biol. 97: 795–802.

8. Bengtsson, A., L. Joergensen, T.S. Rask, R.W. Olsen, M.A. Andersen, L. Turner, T.G. Theander, L. Hviid, M.K. Higgins, A. Craig, A. Brown, and A.T.R. Jensen. 2013. A Novel Domain Cassette Identifies Plasmodium falciparum PfEMP1 Proteins Binding ICAM-1 and Is a Target of Cross-Reactive, Adhesion-Inhibitory Antibodies. J. Immunol. 190: 240–249.

9. Blythe, J.E., X.Y. Yam, C. Kuss, Z. Bozdech, A.A. Holder, K. Marsh, J. Langhorne, and P.R. Preiser. 2008. Plasmodium falciparum STEVOR proteins are highly expressed in patient isolates and located in the surface membranes of infected red blood cells and the apical tips of merozoites. Infect. Immun. 76: 3329–36.

10. Singh, H., K. Madnani, Y.B. Lim, J. Cao, P.R. Preiser, and C.T. Lim. 2017. Expression dynamics and physiologically relevant functional study of STEVOR in asexual stages of Plasmodium falciparum infection. Cell. Microbiol. 19: e12715.

11. Kyes, S.A., J.A. Rowe, N. Kriek, and C.I. Newbold. 1999. Rifins: a second family of clonally variant proteins expressed on the surface of red cells infected with Plasmodium falciparum. Proc. Natl. Acad. Sci. U. S. A. 96: 9333–8.

12. Kraemer, S.M., and J.D. Smith. 2006. A family affair: var genes, PfEMP1 binding, and malaria disease. Curr. Opin. Microbiol. 9: 374–380.

13. Udomsangpetch, R., B. Pipitaporn, K. Silamut, R. Pinches, S. Kyes, S. Looareesuwan, C. Newbold, and N.J. White. 2002. Febrile temperatures induce cytoadherence of ring-stage Plasmodium falciparum-infected erythrocytes. Proc. Natl. Acad. Sci. U. S. A. 99: 11825–9.

14. Spycher, C., M. Rug, N. Klonis, D.J.P. Ferguson, A.F. Cowman, H.-P. Beck, and L.

Tilley. 2006. Genesis of and Trafficking to the Maurer's Clefts of Plasmodium falciparum-Infected Erythrocytes. Mol. Cell. Biol. 26: 4074–4085.

15. Spycher, C., M. Rug, E. Pachlatko, E. Hanssen, D. Ferguson, A.F. Cowman, L. Tilley, and H.-P. Beck. 2008. The Maurer's cleft protein MAHRP1 is essential for trafficking of PfEMP1 to the surface of Plasmodium falciparum-infected erythrocytes. Mol. Microbiol. 68: 1300–1314.

16. Ch'ng, J.-H., M. Sirel, A. Zandian, M. del Pilar Quintana, S. Chun Leung Chan, K. Moll, A. Tellgren-Roth, I. Nilsson, P. Nilsson, U. Qundos, and M. Wahlgren. 2017. Epitopes of anti-RIFIN antibodies and characterization of rif-expressing Plasmodium falciparum parasites by RNA sequencing. Sci. Rep. 7: 43190.

17. Niang, M., A.K. Bei, K.G. Madnani, S. Pelly, S. Dankwa, U. Kanjee, K. Gunalan, A. Amaladoss, K.P. Yeo, N.S. Bob, B. Malleret, M.T. Duraisingh, and P.R. Preiser. 2014. STEVOR Is a Plasmodium falciparum Erythrocyte Binding Protein that Mediates Merozoite Invasion and Rosetting. Cell Host Microbe. 16: 81–93.

18. Lim, Y.B., J. Thingna, J. Cao, and C.T. Lim. 2017. Single molecule and multiple bond characterization of catch bond associated cytoadhesion in malaria. Sci. Rep. 7: 4208.